Progress In Electromagnetics Research, PIER 79, 225–250, 2008

DEVELOPMENT OF A MODEL FOR DETECTION AND ESTIMATION OF DEPTH OF SHALLOW BURIED NON-METALLIC LANDMINE AT MICROWAVE X-BAND FREQUENCY

K. C. Tiwari

Department of Civil Engineering (Geomatics)
IIT Roorkee, Roorkee, 247667, India

D. Singh

Department of Electronics and Computer Engineering
IIT Roorkee, Roorkee, 247667, India

M. K. Arora

Department of Civil Engineering (Geomatics)
IIT Roorkee, Roorkee, 247667, India

Abstract—Detection and estimation of depth of shallow buried landmines using microwave remote sensing is a complex and computationally intensive task. Despite a lot of research to correctly locate and identify the buried landmines, and to estimate its depth using microwave remote sensing data which is essential for demining with minimal risk, a lot of uncertainties still exist. Therefore in this paper, an extensive study using a ground based X-band scatterometer for detection of shallow buried landmine and estimation of its depth has been carried out. An experimental setup consisting of a ground based scatterometer operating in microwave X-band (10 GHz, 3 cm) has been used to generate backscatter data in a grid of 24×24 and a series of experiments under laboratory conditions conducted using dummy landmines (without explosives) buried to different depths up to 10 cm in dry smooth sand. It is difficult to detect the buried landmine by visual inspection of the raw data; therefore a novel approach by fusion of image processing techniques with electromagnetic (EM) analysis has been evolved for detection and estimation of depth of the landmine. The raw data generated through the experiments was processed through a series of image processing steps and a

region of interest segmented using Otsu and maximum entropy based thresholding methods for further processing. A detection figure test has been proposed at this stage to reduce false alarms. Genetic algorithm (GA) with an electromagnetic (EM) model fusion has been proposed to estimate the depth after segmenting a suspected region containing the mine. The main advantage of the proposed model is that it does not have any requirement of separate training and test data set to train the optimizer and validate the results. Analyses of the results indicate that it is possible to segment suspected region of interest containing the landmines in data obtained in microwave X-band using either of the two thresholding methods. The depth of buried landmines estimated using the proposed GA optimized EM model was also found to be in good agreement with the actual depth. The proposed analysis is expected to be extremely useful in future in detection and estimation of the depth of landmines using satellite data in microwave X-band.

1. INTRODUCTION

Landmine detection is both a military and humanitarian requirement as thousands of soldiers and innocent civilians are killed or maimed annually due to buried landmines scattered all over the world in conflict/non-conflict zones [1, 2]. Both the western and the northern borders of India which have experienced serious conflicts in the past still have several abandoned, unrecovered and unmarked minefields/mines.

The basic demining process requires physical prodding of the earth to locate the mine and its subsequent removal which is highly risky. The risk is sought to be minimized by introducing an electromagnetic (EM) imaging equipment which generates backscatter data of the suspected region and concurrently processes it to detect the presence of landmine. Land or vehicle based ground penetrating radars (GPRs) are an example of this method. Detection and removal of landmines however is complicated by variety in types of mines, soil types, scattering from layered media, vegetation *etc.* Most detection methods attempt to exploit the dielectric contrast between various intermediate mediums such as air, different layers of soil and the mine [3]. Landmines are often laid flush with the ground or at shallow depths and have little or no metal content. Hence the dielectric contrast between the layered soil medium and the mine overlaps with the dielectric contrast existing at the air-ground surface which results in diminished backscatter response form the mine thereby making

its detection extremely difficult [3, 4]. Landmine detection therefore poses two main challenges in detecting small shallow buried landmines which contain little or no metal i.e., soil clutter reduction and mine feature extraction. Further, minefields are often laid spread over a large area and therefore the utility of ground or vehicle based methods for the landmine detection task may be limited [4]. Microwave radar remote sensing with subsurface penetration and capability to resolve landmines as well as non-lethal targets is a very encouraging field of research and provides a good alternative for landmine detection with many advantages over ground and vehicle based techniques [3]. The detection process in this case is entirely risk free and it is possible to scan large parts of the conflict zone simultaneously thus providing real time information for operational planning.

Various signal and image processing algorithms are under development world over to accurately solve the mine detection problem. Some signal processing methods search for the hyperbola characterising the landmine response so as to determine the presence of landmines as also to predict its geometry and depth [5]. Neural networks have been used to reconstruct geometric and dielectric characteristics of buried objects [6]. Four signal processing techniques that incorporate features derived from simple physics based sensor models, a generalized likelihood ratio technique, a maximum likelihood estimation based clustering algorithm, a probabilistic neural network and a subtractive fuzzy clustering technique have been applied on data generated through field measurements in a magnetically clean pit and it was found that subtractive fuzzy technique performs better when the training and testing data sets are separate [7]. The buried object detection problem has also been addressed by recasting it into a regression estimation problem and successively solved by means of a support vector machine (SVM) [8]. Markov random models have been used to model the signal returns from landmines and backgrounds and estimate the likelihood that the signal returns are from the landmines [9]. They have also been found to give higher detection performance with incorporation of *a priori* knowledge of spatial structure of the buried object. Statistical approaches such as combining high dimensional analysis of variance and sequential probability ratio test (SPRT) to detect buried objects by exploiting the transient characteristics of the GPR in time domain too has been reported [10, 19–26].

In most of the research however, the electromagnetic interactions at the air-ground-landmine surface has not been modeled due to the complexities involved. Some researchers have attempted to analyse the problem but modeled it differently. A numerical model has been applied in a Monte Carlo study of scattering from a three dimensional

penetrable object below a lossy dielectric surface, both in time and frequency domain to investigate the relative importance of coherent and incoherent scattering effects [11]. A theoretical model using microwave remote sensing in P-band (441 MHz, 68 cm) for buried reflectors at depth H has also been evaluated and the results have been well supported by the experimental investigations conducted in Negev Desert [12]. Ulaby et al. [13] have also proposed a relationship between radar observation depth as a function of observation frequency and soil moisture content by considering the power of an electromagnetic wave incident upon a soil surface [13].

However despite extensive research for detection and estimation of the depth, either the models developed are complex and computationally intensive or there is a requirement of some *a priori* information. Therefore in the present paper, a novel approach by fusion of image processing techniques with electromagnetic (EM) analysis has been evolved for detection and estimation of depth of the landmine. Landmines are often buried to shallow depths at which microwave X-band may have adequate subsurface penetration to resolve the mine [3]. Therefore raw data has been generated in microwave X-band buried in sand and a suspected region containing the mine segmented using image processing techniques. A detection figure test has been proposed at this stage to reduce false alarms. For estimation of the depth, an electromagnetic (EM) model has been proposed for development of fitness function which has been optimized using genetic algorithm. The main advantage of the proposed model is that it does not have any requirement of separate training and test data set to train the optimizer and validate the results. The paper is divided in five sections. Section 2 describes the experimental setup and Section 3 gives both the theoretical modeling and the implementation steps. Section 4 provides the results and the discussions followed by conclusions in Section 5.

2. EXPERIMENTAL SETUP

A scatterometer consists of a transmitter, a receiver, an antenna, and an electronics system to process and record the data. The transmitter generates successive short bursts (or pulses of microwave at regular intervals which are focused by the antenna into a beam towards the target. The radar beam illuminates the surface. The antenna receives a portion of the transmitted energy reflected (or backscattered) from various objects within the illuminated beam. By measuring backscattered "echo" from different targets, an image of the surface can be generated. In case a single antenna with the help of a circulator is used for both the transmission of the microwave signal as well as for

its reception, it is called a monostatic scatterometer.

A set of experiments have been conducted with dummy landmines without explosives buried in sand for detection and estimation of it depth. The experiments have been conducted using an indigenously developed monostatic scatterometer. The schematic layout of the indigenously developed monostatic scatterometer system is given in Figure 1. The system consists of one pyramidal horn antenna connected through a circulator to microwave transmitter on one side and power meter on the other. An isolator giving an isolation of 35 dB has been used to generate experimental data in both HH and VV polarizations. A wooden box measuring 120 cm by 120 cm in size has been created and filled with dry sand for mines to be buried. The height of the base of X-band antennae from the surface is 100 cm. The system has provision to move the antennae in both X and Y directions. The horizontal bars on the two sides (called X-Y direction) have been marked serially in steps of 5 cm from 1 to 24 to make a grid. The circulator and the antenna are moved laterally (Y-direction) from 1–24 at each of the horizontal (X-direction) positions from 1 to 24 for collection of data, thus making a total of 24×24 positions.

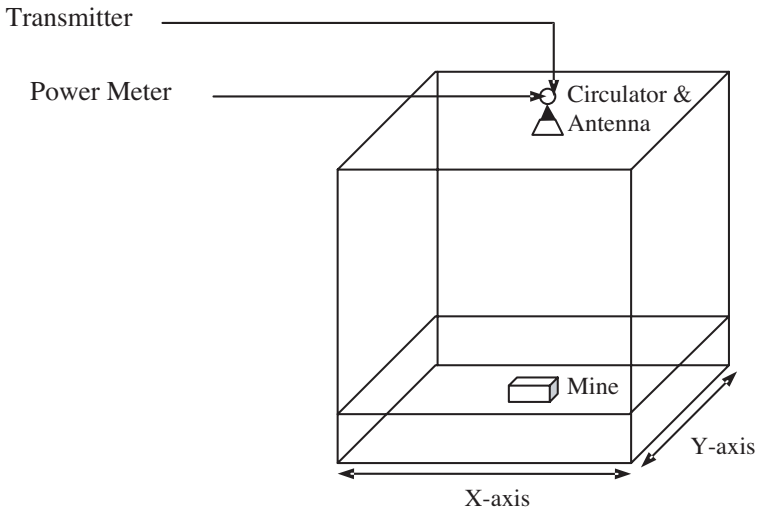

Figure 1. Schematic diagram of monostatic scatterometer system.

For the experiments, three dummy landmines without explosives namely dummy antitank, dummy fragmentation and dummy influence mines have been used. The details of these landmines are given in Figure 2 below. The dielectric constant of these dummy landmines without explosives was assumed to be in the range of 4–10 and the

Dummy/Live	Dummy Mines		
Mine Type	Anti tank Mine	Fragmentation Mine	Influence Mine
Image	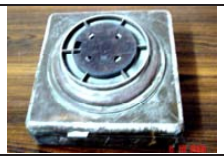		
(a)		(b)	(c)
Dimensions (cm),Wt (kgs)	L=25 cm, W=25 cm, H=7 cm, Wt =7 kgs	Dia -10 cm Ht=12 cm Wt = 3.6 kgs	L=27 cm, W= 18 cm, H=10 cm, Wt =7 kg

Figure 2. Details of mines used in the experiments.

dielectric constant of smooth dry sand was taken to be in the range of 3–5 [13].

Monostatic scatterometer was indigenously developed in the lab at X-band to conduct the experiments. Backscatter readings were recorded at an interval of 0.5 cm from 0.5 cm to 3.0 cm, and thereafter at an interval of 1.0 cm from 4.0 to 10 cm. While discussing microwave energy, the polarization of the radiation is also important. Polarization refers to the orientation of the electric field. Scatterometers are often designed to transmit and receive microwave radiation either horizontally polarized (H) or vertically polarized (V). Accordingly, the data was generated in both HH and VV polarizations keeping both the transmit and the receive polarizations same. Thus a total of twenty different experiments per landmine were conducted. The complete design of experiments has been summarized in Table 1. The dummy landmine in all the experiments was kept at the centre of the box. The raw backscatter reading was calibrated using an aluminum sheet which has a conductivity of 3.5×10^7 Seimens per meter and which

Table 1. Summary of design of experiments.

Detail	Dummy Mines
Location of Setup	Laboratory
Microwave Frequency Band	X-Band only
Medium and Moisture Condition	Dry Sand
Polarisation	HH and VV
Location of Mine	Buried at the Center at different Depths
Mines used in the Experiments	Dummy Antitank, Fragmentation, Influence Mine
Smooth Surface, Depth (cm)	0.5. 1.0, 1.5, 2.0, 2.5, 3.0, 4, 5, 7, 10
Number of experiments to collect data	60 experiments
Experiments with mixed mines	01 (with all the four mines)

is assumed to be a perfect reflector (reflectivity coefficient ≈ 1). An aluminum sheet of the size of the sand pit was placed over the sandpit and backscatter readings noted for the complete 24×24 array. The backscatter readings with buried landmines at different depths were divided pixel by pixel by the corresponding readings taken for the aluminum sheet.

3. MODELLING AND IMPLEMENTATION

This section briefly discusses the theoretical approach which has been used to develop the model and the implementation steps for detection and depth estimation of the landmine. The necessary codes for the implementation of the above model were generated in MATLAB using the image processing and Genetic Algorithm toolboxes.

Choice of frequency is an important parameter in microwave radar remote sensing for detection of buried landmines/objects because of the conflict between the need for ground penetration and for tolerable ground resolution. Lower frequencies penetrate higher, while higher frequencies resolve better. Landmines are often laid flush with the ground at shallow depths at which microwave X-band at 10 GHz, 3 cm may provide adequate penetration and ground resolution [3]. Further at this band, the volume scattering from inhomogeneities of the layered media (small rough surfaces such as in sand layer) can be ignored because of the dimensions of inhomogeneous particles and the distance between them is of the order of 2.5×10^{-3}, both of which are much smaller than the wavelength [12]. All experiments in this study have therefore been conducted in microwave X band region with dummy landmines without explosives buried in dry sand with surface roughness conditions assumed as smooth. Experimental data was generated in HH and VV polarization for different mines buried at different depths. The raw data thus generated was processed through the proposed model for detection and estimation of depth. A flow chart of the implementation steps of the proposed model are given in Figure 3.

3.1. Image Processing for Mine Feature Extraction

The microwave backscatter electrical field depends upon the dielectric properties of the intermediate interacting mediums. The presence of high dielectric contrast at the air-soil interface as compared to low dielectric contrast at the soil - mine interface results in high soil clutter and attenuation of desired backscatter signals from the mine surface [3]. All forms of undesired signals require estimation and subsequent removal in order to enhance the target signal. A common method for

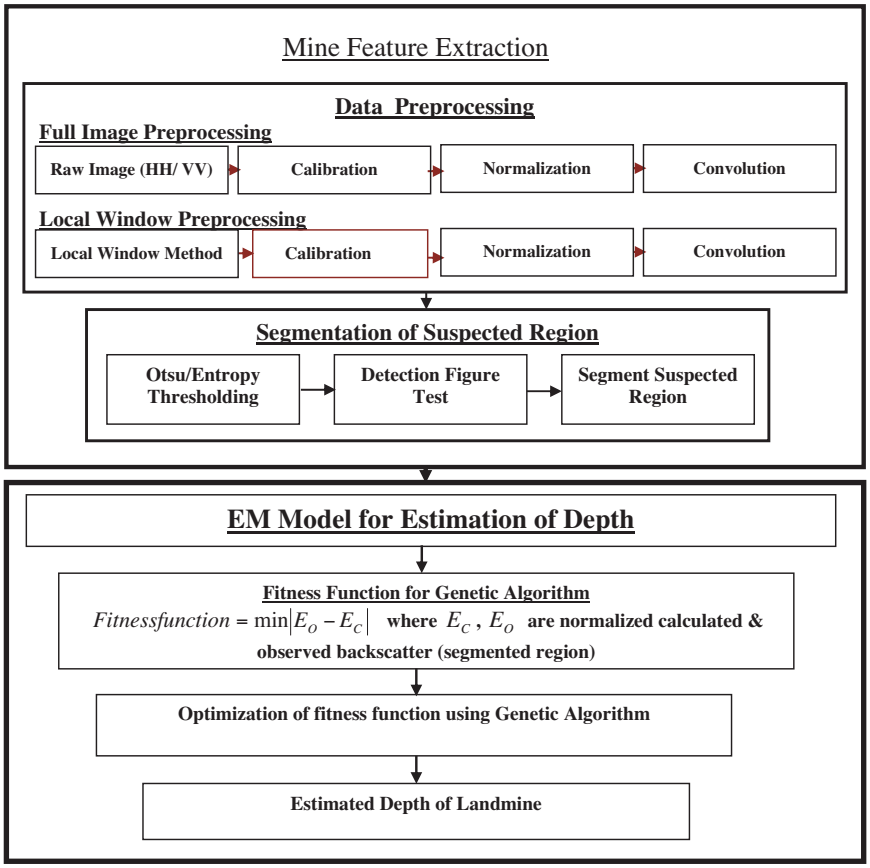

Figure 3. Flow chart of the implementation steps of the model.

clutter reduction is to simply compute the mean vector and subtract this value from individual pixel reading. This method however fails in case the contour of the ground surface is not smooth [14]. The aim of mine feature extraction is to classify a signal into mine or non-mine features and to make a decision between the two during post processing and extract the features containing the landmine. In the present model, a series of steps have been considered for segmenting and masking a suspected region of interest containing the mine. These steps are explained in the following paragraphs

Step -1: Data Preprocessing

Raw data was generated in a grid of 24×24 matrix as discussed earlier. Each grid of 24×24 array was assumed to constitute one pixel.

The raw backscatter reading was calibrated using an aluminum sheet which has a conductivity of 3.5×10^7 Seimens per meter and which is assumed to be a perfect reflector (reflectivity coefficient ≈ 1). An aluminum sheet of the size of the sand pit was placed inside the sandpit and backscatter readings noted for the complete 24×24 array. The backscatter readings with buried landmines at different depths were divided pixel by pixel by the corresponding readings taken for the aluminum sheet. The raw image were calibrated and after that normalized using the following equation [12]:

$$E_{normalised} = \frac{E_{observed} - E_{\min}}{E_{\max} - E_{\min}} \tag{1}$$

where $E_{\max}$ and $E_{\min}$ are the maximum and minimum values in the observed data, $E_{observed}$ is the backscattered intensity at particular point. The normalization has been done to put all the data in one range. The illumination area of the antenna system is not limited to the pixel size of the image, so there is a significant contribution from the neighboring pixels. Therefore, to minimize the effect of overlap of the scattered field from neighboring pixels and to reduce the effect of random noise spikes, an optimized 5×5 convolution kernel filter was applied to all the images. The convoluted data was then assumed pure reading per pixel [15]. It may however be pointed out that selection of an appropriate convolution filter would depend upon the antenna and the microwave frequency band being used.

Two different approaches have been considered for data preprocessing namely, full image data preprocessing and local window data preprocessing which are described below

(i) **Full image Data Preprocessing** - In this case, the complete raw image generated in the experiments is subjected through the series of data preprocessing steps enumerated above without subjecting it to any other image processing task. The advantage of this method is that it results in analysis of actual raw backscatter image. However, in the case of subsurface landmine where the backscatter from the landmine may not show any significant variation from the surroundings, this method may lead to loss of mine features.

(ii) **Local Window Data Preprocessing** - Mine feature extraction requires discrimination between mine like features from the non-mine like features in a complex background. Due to limited dielectric variations between the landmine and the medium in which it is buried, clutter arising from dielectric contrast at various medium interfaces, clutter due to surface roughness and the small size of the landmine, the backscatter response from the landmine

in a scatterometer measurement is usually restricted to a limited number of pixels only. Under these circumstances, in order to identify pixels containing the mine like features, processing in a local window may be more useful. Following procedure has been adopted

(a) First, a new image is generated by multiplying an identity matrix of the same size as the raw image with the mean backscatter value of the raw image. A three dimensional plot of this image is a flat image with its height equal to the mean backscatter value. Further, since the backscatter from the landmine may be lower than the this mean backscatter, the new image is further scaled down by multiplying it by a fraction in the range of 0.5 to 0.8, the exact value of which is determined by trial and error in each experiment.

(b) The raw image is then divided into several blocks of smaller windows and at a time, one of these windows is transferred to its corresponding position in the new image and the new image processed through various data preprocessing steps outlined earlier. An optimal size of window depends upon the expected size of the mine, resolution, likely presence of other objects in the surroundings and the clutter. In the present case, a size of 8×8 pixels window was considered sufficient, however greater window sizes should be preferred as this may speed up the processing.

Step -2: Mine Feature Extraction

Mine feature extraction involves segmenting a suspected region containing landmines and a test to reduce false alarms. Because of simplicity of implementation, thresholding is a commonly adopted method to segment an image to obtain the suspected area where an object may be buried. Selection of a proper threshold value is however important in correctly detecting an object. Otsu's and entropy based thresholding methods have commonly been reported in the literature [16, 17]. The convoluted data obtained for each of the mines at different depths was analysed using these two thresholding techniques for extraction of the mine features. The two thresholding methods are discussed here briefly.

Otsu's method [16] provides a method to set a threshold so as to try to make each cluster as tight as possible. It aims at minimizing the within class variance and maximizing the between class variance. This histogram based method can be understood by treating the normalized histogram as a discreet probability density function, as in

$$p_r(r_q) = \frac{n_q}{n} \tag{2}$$

where $q = 0, 1, 2 \ldots L-1$, n is the total number of pixels in the image, n_q is the number of pixels that have intensity level r_q, and L is the total number of possible intensity levels in the image. If a threshold is chosen such that it thresholds the image into two segments, Otsu's method chooses the threshold such that it minimizes the within class variance and maximizes the between class variance.

On the other hand, maximum entropy principle serves as a criterion to select *a priori* probability distributions when very little or nothing is known. It states that, for a given amount of the information, the probability distribution which best describes our knowledge is the one that maximizes the 'Shannon entropy' subject to the evidence given as constraints [17]. After thresholding an image with threshold t, a bi-level image is obtained. The *a posteriori* probability of the pixels with gray values less than the threshold is given by equation (3).

$$F(t) = \sum_{i=0}^{t} p_i \tag{3}$$

Similarly, the *a posteriori* probability of all those pixels with values greater than or equal to t is $(1 - F(t))$. Thus, the Shannon entropy of the bi-level image is given by equation (4).

$$H(F(t)) = -F(t) \log F(t) - (1 - F(t)) \log(1 - F(t)) \tag{4}$$

If nothing else is known then an optimal threshold is obtained by maximizing the Shanon entropy of the bi-level image. However, the histogram of the image may not be bi-modal always and other information regarding the image such as uniformity measure or shape measure *etc.* may have to be incorporated.

Detection Figure Test - Any detection has to be robust enough to produce as little false alarms as possible. Suitable detection accuracy measures must therefore be incorporated to predict detections which are immune to noise and background illumination. For reduction of false points, a quantity detection figure (D) test based on image statistics has been developed to assess the correctness of detection. The detection figure test is applied on the thresholded data and is based on the mean intensity of foreground pixels (those pixels for which reading is above or equal to threshold) and the mean intensity of the whole data. The detection figure (D) can be defined as

$$\text{Detection figure } (D) = \frac{A(FG) - A(BG) \times 100}{A(FG + BG)} \tag{5}$$

where, $A(FG)$ = average reading for foreground pixels, $A(BG)$ = average reading for background pixels and $A(FG + BG)$ = average reading for all pixels.

The detection figure has been calculated for different depths of dummy landmine. When there is no object buried into sandpit all readings represent backscattering from sand, hence difference between $A(FG)$ and $A(BG)$ will be small and detection figure will have a small value. It was found that if detection figure obtained is less than 40, we could claim that there is no object buried in sand. However, detection figure values were found to lie in the range from 40 to 80 for correct detections.

Step -3: Segmentation and Masking of Region of Interest

Once the detection figure test indicated correct detection, the segmentation provided by the thresholding was used to mask the suspected region retaining the original backscatter values in the region. The average of the backscatter for this suspected region for any given depth was treated as input to the proposed GA optimized EM model described next for estimation of depth.

3.2. Proposed Genetic Algorithm Optimized Electromagnetic (EM) Model for Estimation of Depth

The interaction of an electromagnetic wave with soil is a complex phenomenon. Figure 3 gives a schematic diagram of electrical field propagation for subsurface penetration as in the present case.

The total returned electrical field received at the scatterometer end E_R is the result of simultaneous specular reflection and diffuse scattering at the air-sand interface, reflection from the mine buried at depth H, diffraction and scattering by surface irregularities of the reflector and volume scattering from the sand layer [12]. The total returned field E_R at the scatterometer receiver due to the mine buried at depth H is given by (Figure 4)

$$E_R = E_s + E_{c1} + E_{c2} + E_{c3} + \ldots E_{cn} \tag{6}$$

Daniels et al. [12] have derived the following equation for determination of depth under sand which is being used in the present model

$$E_R = \sqrt{1 - 4k^2\sigma^2 \cos\theta_1 \exp\left(-\frac{1}{2}\sin\theta_1\right)}\,\frac{R_{1-2} + R_{2-3}\exp(-2\gamma_2 H)}{1 + R_{1-2} + R_{2-3}\exp(-2\gamma_2 H)} \tag{7}$$

where $k = 2\pi/\lambda =$ wave No, $\sigma =$ roughness parameters, $\theta_1 =$ incident angle, $H =$ depth

$$R_{1-2} = \frac{\sqrt{\varepsilon_1} - \sqrt{\varepsilon_2}}{\sqrt{\varepsilon_1} + \sqrt{\varepsilon_2}} \qquad R_{2-3} = \frac{\sqrt{\varepsilon_2} - \sqrt{\varepsilon_3}}{\sqrt{\varepsilon_2} + \sqrt{\varepsilon_3}} \tag{8}$$

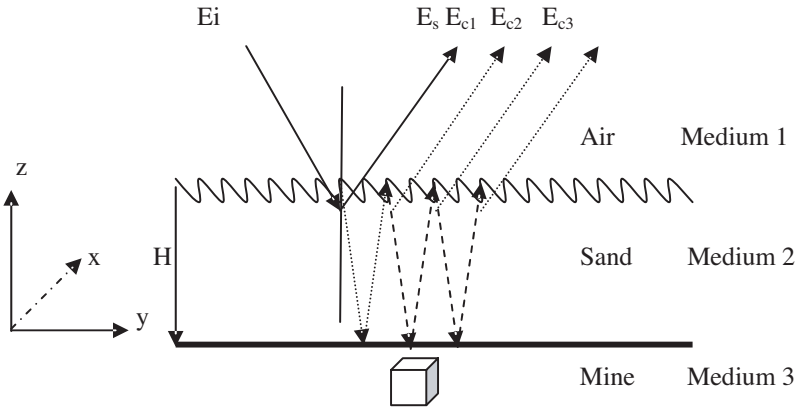

Figure 4. Microwave propagation in an air-soil-mine interface.

(subscripts 1, 2 & 3 refer to first, second & third medium i.e., air, sand and mine)
and the propagation constant γ_2 in second medium i.e., sand is given by

$$\gamma_2 = \frac{2\pi}{\lambda}\sqrt{\varepsilon_2}$$

The estimated average backscatter after segmenting and masking the suspected region of interest and the theoretical backscatter calculated using equation -7 was optimized using Genetic Algorithm (GA). Genetic algorithms are robust optimizers, stochastic search methods modeled on the principles and concepts of natural selection and evolution. GA is effective in solving complex problems. These are particularly effective when the goal is to find global maxima in a high dimension, multi model function domain in a near optimal manner. Genetic algorithm differs from other conventional techniques in the following ways [18]

- They operate on a group (or population) of trial solutions in parallel.
- They operate on a coding of function parameters (chromosomes) rather than on the parameters themselves.
- They use simple, stochastic operators (selection, cross over and mutation) to explore the solution domain in search of an optimal solution.

Successive populations of trial solutions are called generations and subsequent generations i.e. children are produced through selective reproduction of pairs of parents taken from the current generation. The

optimization in genetic algorithms is done through a fitness function (also called cost function or object function) which is used to assign a fitness value to each of the individuals in the GA population. The above GA optimized EM model for estimation of depth was implemented as under

Step -1: Fitness Function for Genetic Algorithm

A fitness function for the proposed model for optimization using GA was derived as under

$$Fitness function = \min |E_O - E_C| \tag{9}$$

where E_O = average observed backscatter
E_C = calculated backscatter Electrical field (Eq. (7)).

Step -2: Optimisation of Fitness Function to Predict Depth of Landmine

The fitness function developed as above (Eq. (9)) was minimized for the normalized values of the observed and calculated backscatter using GA for different initial populations to predict the depth of landmine.

4. RESULTS AND DISCUSSIONS

Lab experiments were carried out with three different dummy landmines without explosives (dummy antitank, dummy fragmentation and dummy influence mine) at different depths. The pattern of results for different mines at different depths is approximately the same, hence only selected results have been explained here in this section.

4.1. Effect of Data Preprocessing

4.1.1. Full Image Data Preprocessing

Data preprocessing has been carried out using two different methods namely, full image data preprocessing and local window based data preprocessing. Full image data preprocessing retains the characteristics of the original data and hence, first the raw data obtained in the laboratory for three different dummy mines at different depths was processed through various data preprocessing steps namely, calibration, normalization and convolution. The plots generated for raw data, calibrated data and convoluted data for each of these three mines at a depth of 1.5 cm are shown in Figures 5(a) to (i). The aim of data preprocessing is to process the image to an extent at which

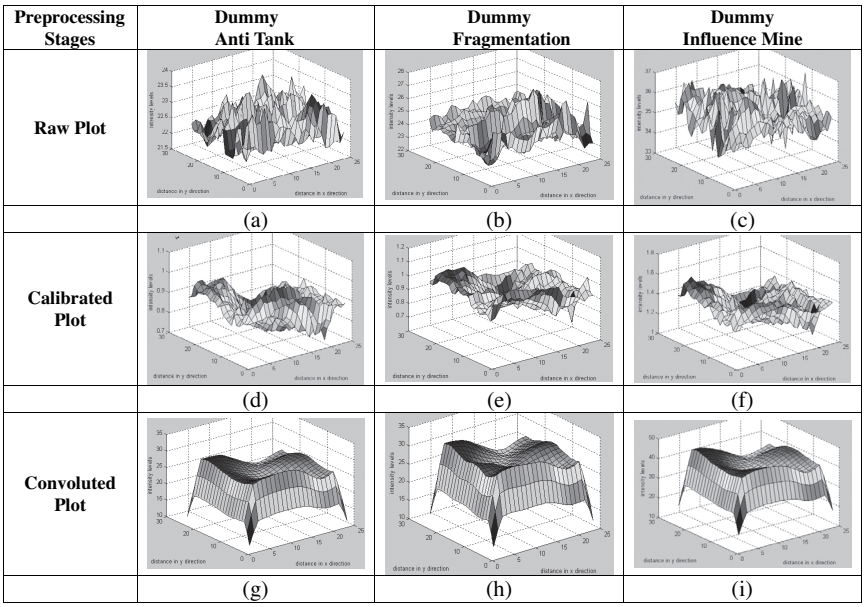

Figure 5. Plots at different stages of full image data preprocessing at depth of 1.5 cm (VV polarisation) (x and y axes - dimensions of the image, z axis - backscatter intensity).

extraction of desired attributes from the image become feasible. It is noticed that the plots for the raw data (Figures 5(a) to (c)) is highly random due to clutter from various sources including that from the corner of boxes. Data preprocessing after calibration is shown in Figures 5(d) to (f) and after convolution in Figures 5(g) to (i). It is noticed that data preprocessing in this manner results in a smoothened image with noise around the corners severely restricted. A minor dip in all the convolution plots towards the centre is noticed. Thus the convolution plot for all the mines at all the depths highlighted the likely area containing the mines which in these experiments was kept at the centre.

4.1.2. Effect of Local Window based Data Preprocessing

The dielectric variations due to mine in the presence of clutter are likely to get reflected in only a few pixels. The aim of data preprocessing is to transform the raw data so as to minimize the clutter and highlight the mine like features and facilitate segmentation of suspected region containing the mine during the post processing stage. The results

Data Preprocessing	Dummy Anti Tank Mine	Dummy Fragm-entation Mine	Dummy Influence Mine
3-D plot of convoluted data	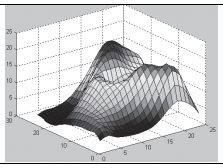	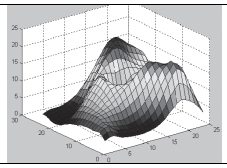	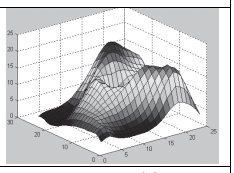
	(a)	(b)	(c)

Figure 6. Effect of local window processing at depth of 1.5 cm (VV polarisation) (x and y axes - dimensions of the image, z axis - backscatter intensity).

with full image data preprocessing indicated that preprocessing with full image possibly leads to redistribution of clutter present in the image thereby making discrimination of mine features more difficult. The segmentation using thresholding methods in such cases are likely to yield incorrect results. To overcome this problem, local window based data preprocessing as explained earlier was adopted. In this case, barring a small window, rest of the image is suppressed below the mean backscatter value of the image. It produces a zooming effect for the window selected and results in a preprocessed image in which mine like and non mine like features are easy to segment. The results of local window based data preprocessing at the end of convolution stage is shown in Figures 6(a) to (c). These results can be compared with the results shown in Figures 5(g) to (i). It has a clear dip at the centre indicating a variation in backscatter in that region. It was thus found that the local window processing yields significantly better results and makes it possible to accurately segment the suspected region containing the landmines.

4.2. Segmentation Using Otsu's and Maximum Entropy Based Thresholding

The suspected region containing the mines was segmented using Otsu's and the maximum entropy based thresholding methods. The results of the segmentation using Otsu's thresholding for the three mines are shown in Figures 7(a), (b) and (c). Similarly, the results of the segmentation using maximum entropy based thresholding for the three mines are shown in Figures 7(d), (e) and (f). It is however not possible to determine the difference between the two methods purely by a visual inspection of the segmentation results, hence these were analysed using threshold values determined by each of the two

Thresholding method	Dummy Anti Tank Mine Depth 1.5 cm	Dummy Fragmentation Mine Depth 1.5 cm	Dummy Influence Mine Depth 1.5 cm
Otsu's thresholding method		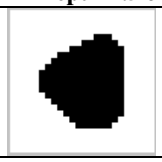	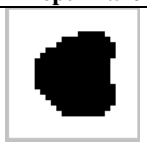
	(a)	(b)	(c)
Maximum entropy based thresholding			
	(d)	(e)	(f)

Figure 7. Segmentation results using Otsu's/ maximum entropy based thresholding methods (VV polarisation).

thresholding methods, the detection figures obtained and the number of pixels segmented. The Otsu's thresholding method results in threshold values in the range of 101 to 108. 50 and the detection figure in the range of 51.46 to 61.33. In comparison, maximum entropy based thresholding results in threshold values in the range of 98.60 to 106.79 and detection figures in the range of 51.05 to 61.94. The threshold values and the detection figures obtained for dummy antitank mine in VV polarization were plotted together as shown in Figure 8. It was noticed that the thresholding using maximum entropy based method yields threshold values lower than the Otsu's threshold values except at the depth of 7 cm. This also gets reflected in the corresponding detection figures which are also lower. Together, it indicates higher accuracy of segmentation. This further gets reinforced by counting the number of pixels segmented by each of the two thresholding methods. The total numbers of pixels in the image are $24 \times 24 = 576$ pixels. The minimum number of pixels segmented at depth 1.5 cm for fragmentation mine using Otsu's method is 362 (refer Figure 7(b)) while for the maximum entropy based method, it is 347 (refer Figure 7(e)). The difference in these numbers is higher at all depths and for all other mines, however the maximum difference between the two does not exceed a maximum of 5%.

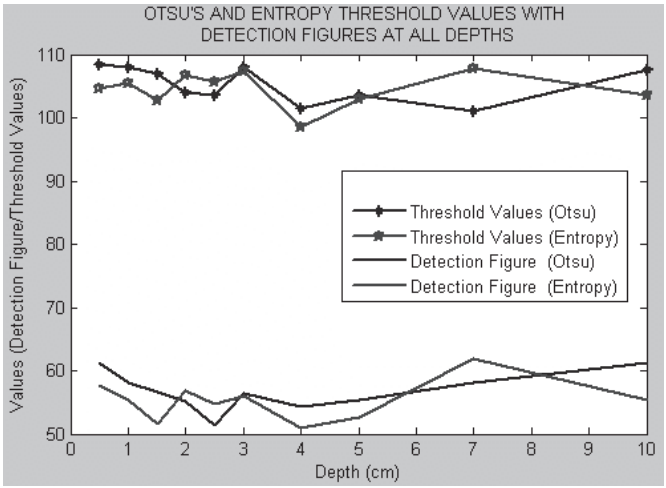

Figure 8. Otsu's and maximum entropy based threshold values with detection figures (dummy antitank mine in VV polarisation).

4.3. Effect of Polarization on Segmentation

For all the mines, the respective minimum, maximum and mean values of the data in HH and VV polarization indicated the two data lies in two different ranges. In each case the backscatter for the VV polarization was found to be higher. The standard deviation in the case of VV polarization was higher than that for HH polarization which was indicative of the fact that it had higher discriminating features. This highlighted the requirement of data normalization during the preprocessing stage. Skewness is the third statistical moment and measures asymmetry in data. A negative skewness indicates that the data is skewed to the left of mean and a positive value indicates asymmetry in the other direction [11]. Data in both the polarizations were found to be skewed to the left, however the data in VV polarization had higher skewness. Similarly, Kurtosis is another statistical moment of fourth order and is known to be outlier sensitive. Kurtosis of a normal distribution is 3, those distributions which are more outlier prone have kurtosis value greater than 3 and those which are less outlier prone have kurtosis value less than 3 [11]. The data in each polarization had a Kurtosis value less than 3 but the data in VV polarization had a higher kurtosis value than that of HH polarization. Further data preprocessing leads to increase in these values marginally thereby aiding the discrimination further. The analysis of these two statistical moments imply that data in

Operation	Antitank Mine at Depth 1.5 cm		Fragmentation Mine at Depth 1.5 cm	
Polarisation	HH Polarisation	VV Polarisation	HH Polarisation	VV Polarisation
Entropy Thresholding Detection	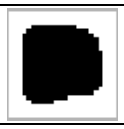	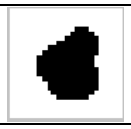	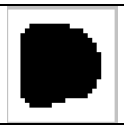	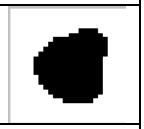
	(a)	(b)	(c)	(d)
Detection Figure	54.87	59.27	53.56	61.73
Figure 9 - Effect of Polarisation on segmentation				

Figure 9. Effect of polarization on segmentation.

HH and VV polarizations contain different levels of information, skewness away from mean indicated likely presence of some object though low outlier sensitivity indicates little variation within the data distribution. Further, the segmentation in each of the two polarization is given in Figures 9(a) and (b) for antitank mine and Figures 9(c) and (d) for fragmentation mine respectively. It is noticed that although the thresholded values may indicate the likely location of the mine, but there is enough backscatter in the same thresholded range due to clutter/noise. Further, the number of pixels segmented may not correctly indicate the true mine pixels due to either residual antenna overlap or clutter. It is possible that most of the clutter may lie entirely in the same range as the mine features and may lead to failure of either of the thresholding methods. Though in such cases, entropy based methods which introduces constraints of uniformity and shape *etc.* are likely to perform well but still there is a need to improve data preprocessing for an accurate segmentation at post processing stage.

4.4. Effect of Local Window based preprocessing on Segmentation

The effect of local window based data preprocessing has been discussed in the previous subsection. In this section, the discussion is extended to segmentation achieved using local window based data preprocessing. Figures 10(a) and (c) show the segmentation for dummy antitank mine in both the polarizations when full image data preprocessing is been carried out. In comparison when the local window based data preprocessing is carried out, it yields significantly better results as shown in Figures 10(b) and (d).

In order to validate the usefulness of local window based data

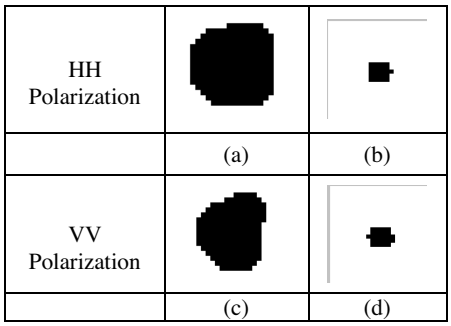

Figure 10. Effect of local window data preprocessing on segmentation for dummy antitank mine at depth of 1.5 cm.

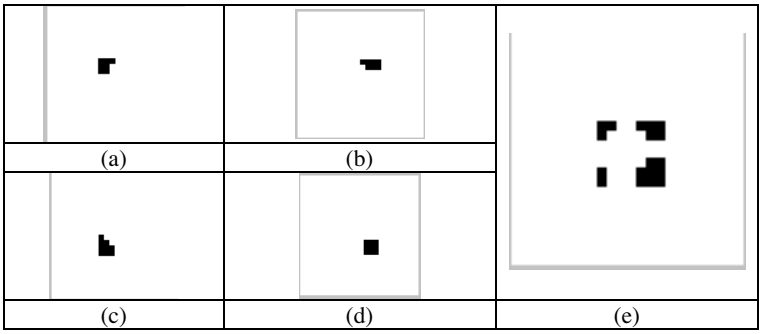

Figure 11. Segmentation achieved with all four mines buried in square pattern (HH polarization).

preprocessing, one set of experiment has been conducted with all the four different mines buried simultaneously at a depth of 1.0 cm in a square pattern. All the four mines have been recovered using the local window based data preprocessing in both the polarizations. Figure 11 shows the segmentation achieved for HH Polarization. The result for the VV polarization is also the same. Figures 11(a) to (d) show the result when each of the mines is recovered in independent windows. Figure 11(e) shows the result when all the four windows were combined together before segmentation.

The surface plots after local window based processing and entropy thresholding based detection for all the three mines at a depth of 1.5 cm are given in Figures 12(a) to (l). The segmentation achieved is evidently much superior to any of the previous results. Similar results have been obtained at all depths in both the polarizations.

Results at Depth 1.5 cm				
	Surface Plots – convoluted data		Entropy Thresholding	
Mine	HH Polarization	VV Polarization	HH Polarization	VV Polarization
Antitank Mine	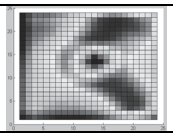	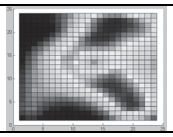	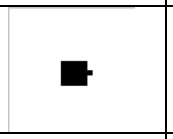	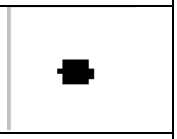
	(a)	(b)	(c)	(d)
Dummy Fragmentation Mine	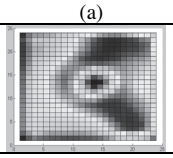	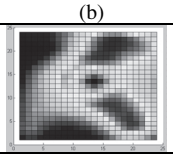	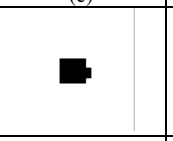	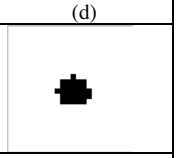
	(e)	(f)	(g)	(h)
Dummy Influence Mine	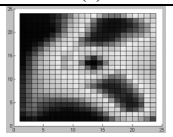	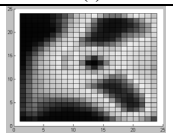	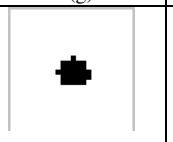	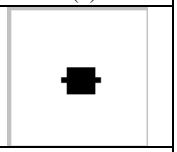
	(i)	(j)	(k)	(l)

Figure 12. Results for various mines with local window data preprocessing in dry smooth sand.

4.5. Detection Figure Test

Detection figures for all the three dummy mines were plotted against depth. The results were found to be generally the same. The plot for dummy antitank mine is shown in Figure 13. From the analysis, the range of detection figures which yielded correct results were found to be from 45–75. Therefore, it was concluded that in case detection figures falls outside 40–80, then there was no landmine/object buried in the background.

4.6. Estimation of Depth

After segmenting the suspected region containing the landmine, a fitness function was formulated as difference of observed backscatter and calculated backscatter. The fitness function was optimized using genetic algorithm for estimation of depth. For this purpose GA tool of MATLAB was run with different initial populations and the optimized results for dummy fragmentation mine are given in Table 2. An error plot for dummy fragmentation mine in VV polarization between actual and the predicted depth is given in Figure 14. It is noticed that

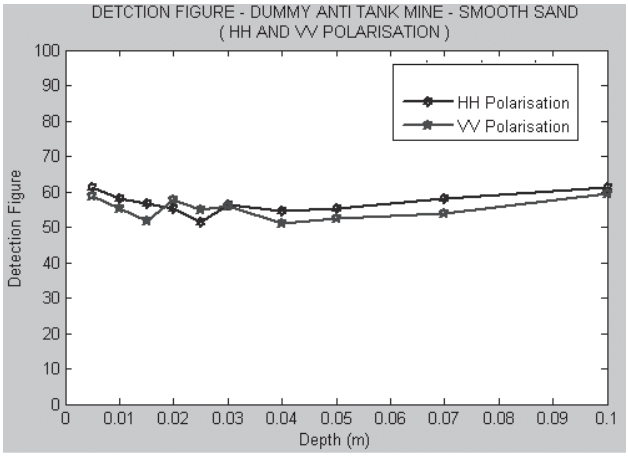

Figure 13. Detection figure plots for dummy antitank mine in dry smooth sand in HH and VV polarizations.

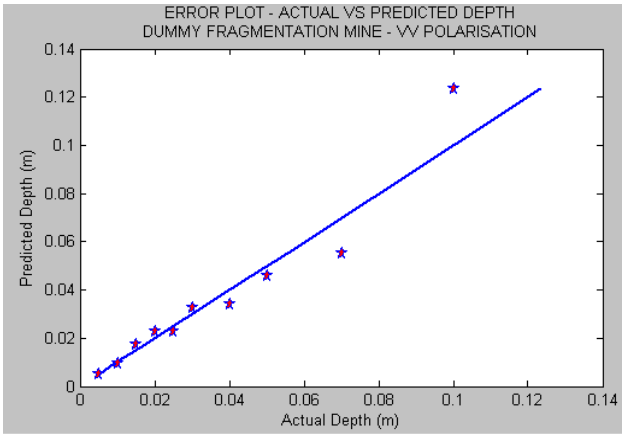

Figure 14. Error plot for depth (actual vs predicted depth) for dummy fragmentation mine.

the error at lower depths showed minor fluctuations but in general increased with the increase in the depth. The results obtained were better at lower and middle depths. In some cases however, the error at initial depths was found to be higher than those at middle depths. Apparently at depths closer to the surface, there is strong interference of soil clutter in the mine backscatter. Similarly with the increase in depth, there is a damping of the electrical field and therefore a

Table 2. Actual and predicted depth for fragmentation mine.

Actual, H	Predicted, P	% Error
0.005	0.006	-21.00
0.01	0.009	+3.60
0.015	0.016	-11.20
0.02	0.023	-18.05
0.025	0.025	-3.32
0.03	0.031	-5.33
0.04	0.034	+14.05
0.05	0.044	+10.08
0.07	0.052	+25.28
0.1	0.135	-35.29

corresponding decrease in backscatter from the mine and increase in the soil clutter. From the figures, it is noticed that the maximum error up to a depth of 7 cm does not exceed 30% of actual depth. Therefore, it may be concluded that the proposed electromagnetic model is capable of predicting the depth correctly subject to the accuracy of the observed backscatter and the content of soil clutter in it. The main advantage of the proposed model is that it does not have any requirement of any *a priori* training data. However, GA based optimization was found to be highly dependent on the choice of initial populations.

5. CONCLUSION

Lab experiments using microwave X-band frequency (10 GHz, 3 cm) has been carried out for subsurface landmine detection and estimation of depth up to a depth of 10 cm. Experimental data was generated with different dummy mines without explosives buried in dry smooth sand at different depths. Raw data was preprocessed through a series of image processing steps and detection was carried out using Otsu's thresholding and the maximum entropy based thresholding methods. The results were validated with the known location of the mines used in the experiments. Performance of the both the thresholding methods were found to be adequate in detection dummy landmines. A detection figure test has been proposed and evaluated for reducing false alarms. The results of detection with data preprocessing was found to be satisfactory and a detection figure in the range of 40–80 was found to

indicate correct detections. An electromagnetic model has also been developed and implemented for estimation of depth of landmine which was optimized using genetic algorithm. GA based optimization of the proposed electromagnetic model also yielded good estimation of depth with the advantage that the model did not have any requirement for *a priori* training or test data. However GA based optimization was found to be highly dependent on the choice of initial populations and it affected the results significantly.

ACKNOWLEDGMENT

The authors are thankful to the Defense Research and Development Organization, Ministry of Defense, India for providing financial support for the project.

REFERENCES

1. Bureau of Political & Military Affairs, "Hidden killers," US Department of State Publication 10575, http:/www.state.gov /www/global/arms/rpt/-9809demineloc.html, September 1998.
2. Potin, D. and P. Vanheeghe, "An abrupt change detection algorithm for buried landmine localization," *IEEE Transactions on Geosciences And Remote Sensing*, Vol. 44, No. 2, Feb. 2006.
3. Maathuis, B. H. P. and J. L. Van Genderen, "A review of satellite and airborne sensors for remote sensing based detection of minefields and landmines," *Intl. Journal of Remote Sensing*, 10, Dec. 2004.
4. Druyts, P., Y. Yvinee, and M. Acheroy, "Usefulness of semi-automatic tools for airborne minefield detection," Signal and Image Centre, Royal Military Academy, Belgium, http://www.sic.rma.ac.be.
5. Gader, P. D. et al., "Recognition technology for the detection of buried landmines," *IEEE Transactions Fuzzy Sys.*, Vol. 9, No. 1, Feb. 2001.
6. Carosi, S. and G. Cevini, "An electromagnetic approach based on neural networks for the GPR investigation of buried cylinders," *IEEE Geosciences and Remote Sensing Letters*, Vol. 2, No. 1, Jan. 2005.
7. Collins. L., et al., "A comparison of the performance of statistical and fuzzy algorithms for unexploded ordnance detection," *IEEE Transactions on Fuzzy Systems*, Vol. 9, No. 1, Feb. 2004.

8. Bermani, E. et al., "An innovative real time technique for buried object detection," *IEEE Transactions on Geosciences and Remote Sensing*, Vol. 41, No. 4, April 2003.
9. Gader, et al., "Landmine detection with ground penetrating radar using hidden Markov models," *IEEE Transactions Geosciences and Remote Sensing*, Vol. 41, No. 4, Jun. 2001.
10. Xu, X., et al., "Statistical method to detect subsurface objects using array ground penetrating radar data," *IEEE Transaction on Geosciences and Remote Sensing*, Vol. 40, No. 4, Apr. 2002.
11. Johnson, J. T. and R. J. Burkholder, "A study of scattering from an object below a rough surface," *IEEE Transactions on Geosciences and Remote Sensing*, Vol. 42, No. 1, Jan. 2004.
12. Daniels, J., et al., "Microwave remote sensing of physically buried objects in Negev desert: Implications for subsurface martiani exploration," *Journal of Geophysical Research*, Vol. 108, No. 48033, 2003.
13. Ulaby, F. T., R. K. Moore, and A. K. Fung, *Radar Remote Sensing and Surface Scattering Emission Theory*, Vols. II & III, Addison Wesley Publishing Company, 1982.
14. Brooks, J. W., "The detection of buried non-metallic anti-personnel landmines," Dissertation submitted at University of Alabama, Huntsville, 2000.
15. Petrou, M. and P. Bosdogianni, *Image Processing — The Fundamentals*, John Wiley & Sons, Inc., New York, USA, 1999.
16. Tian, H., et al., "Implementing Otsu's thresholding process using area-time efficient logarithmic approximation unit," *0-7803-7761-3/03 C 2003 IEEE*, Mar. 2003.
17. Wong, A. K. C. and P. K. Sahoo, " A gray level threshold selection method based on maximum entropy principle," *IEEE Transactions on Systems, Man And Cybernetics*, Vol. 19, No. 4, Aug. 1989.
18. Johnson, M., et al., "Genetic algorithms in engineering electromagnetics," *IEEE Antennas and Propagation Magazine*, Vol. 39, No. 4, Aug. 1997.
19. Chen, X., D. Liang, and K. Huang, "Microwave imaging 3-D buried objects using parallel genetic algorithm combined with FDTD technique," *J. of Electromagn. Waves and Appl.*, Vol. 20, No. 13, 1761–1774, 2006.
20. Van den Bosch, I., "Accurate and efficient modelling of monostatic GPR signal of dielectric targets buried in stratified media," *J. of Electromagn. Waves and Appl.*, Vol. 20, No. 3, 283–290, 2006.

21. Nishimoto, M., S. Ueno, and Y. Kimura, "Feature extraction from GPR data for identification of landmine like objects under rough ground surface," *J. of Electromagn. Waves and Appl.*, Vol. 20, No. 12, 1577–1586, 2006.
22. Pingenot, J., "Full wave analysis of RF signal attenuation in a lossy rough surface cave using a high order time domain vector finite element method," *J. of Electromagn. Waves and Appl.*, Vol. 20, No. 12, 1695–1705, 2006.
23. Chen, H.-T. and G.-Q. Zhu, "Model the electromagnetic scattering from three-dimensional PEC object buried under rough ground by MOM and modified PO hybrid method," *Progress In Electromagnetics Research*, PIER 77, 15–27, 2007.
24. Xue, W. and X.-W. Sun, "Multiple targets detection method based on binary Hough transformation and adaptive time frequency filtering," *Progress In Electromagnetics Research*, PIER 74, 309–317, 2007.
25. Bermani, E. and A. Boni, "A multi source strategy based on a learning by examples technique for buried object detection," *Progress In Electromagnetics Research*, PIER 48, 185–200, 2004.
26. Golestani-Rad, L. and J. Rashed-Mohassel, "Rigorous analysis of EM-wave penetration into a typical room using FDTD method: The transfer function concept," *J. of Electromagn. Waves and Appl.*, Vol. 20, No. 7, 913–926, 2006.